Nitrous oxide inhibition of methanogenesis represents an underappreciated greenhouse gas emission feedback

Yongchao Yin[1,2,3,†], Fadime Kara-Murdoch[1,3,‡], Robert W. Murdoch[1,‡], Jun Yan[1,2,4], Gao Chen[1,5], Yongchao Xie[1,5,§], Yanchen Sun[1,5], Frank E. Löffler[1,2,3,5,6,*]

[1]Center for Environmental Biotechnology, University of Tennessee, Knoxville, TN 37996, United States
[2]Department of Microbiology, University of Tennessee, Knoxville, TN 37996, United States
[3]Biosciences Division, Oak Ridge National Laboratory, Oak Ridge, TN 37831, United States
[4]Key Laboratory of Pollution Control and Environmental Engineering, Institute of Applied Ecology, Chinese Academy of Sciences, Shenyang, Liaoning 110016, China
[5]Department of Civil and Environmental Engineering, University of Tennessee, Knoxville, TN 37996, United States
[6]Department of Biosystems Engineering and Soil Science, University of Tennessee, Knoxville, TN 37996, United States

[*]Corresponding author: Frank E. Löffler, Department of Civil & Environmental Engineering, University of Tennessee, 851 Neyland Drive, 325 John D. Tickle Building, Knoxville, TN 37996 United States. Email: frank.loeffler@utk.edu

[†]Present address: Department of Biology, Antimicrobial Discovery Center, Northeastern University, Boston, MA 02115, United States
[‡]Present address: Battelle Memorial Institute, Columbus, OH 43201, United States
[§]Present address: Department of Chemistry and Biochemistry, University of California, Los Angeles, CA 90095, United States

Abstract

Methane (CH_4) and nitrous oxide (N_2O) are major greenhouse gases that are predominantly generated by microbial activities in anoxic environments. N_2O inhibition of methanogenesis has been reported, but comprehensive efforts to obtain kinetic information are lacking. Using the model methanogen *Methanosarcina barkeri* strain Fusaro and digester sludge-derived methanogenic enrichment cultures, we conducted growth yield and kinetic measurements and showed that micromolar concentrations of N_2O suppress the growth of methanogens and CH_4 production from major methanogenic substrate classes. Acetoclastic methanogenesis, estimated to account for two-thirds of the annual 1 billion metric tons of biogenic CH_4, was most sensitive to N_2O, with inhibitory constants (K_I) in the range of 18–25 μM, followed by hydrogenotrophic (K_I, 60–90 μM) and methylotrophic (K_I, 110–130 μM) methanogenesis. Dissolved N_2O concentrations exceeding these K_I values are not uncommon in managed (i.e. fertilized soils and wastewater treatment plants) and unmanaged ecosystems. Future greenhouse gas emissions remain uncertain, particularly from critical zone environments (e.g. thawing permafrost) with large amounts of stored nitrogenous and carbonaceous materials that are experiencing unprecedented warming. Incorporating relevant feedback effects, such as the significant N_2O inhibition on methanogenesis, can refine climate models and improve predictive capabilities.

Keywords: nitrous oxide, methane, greenhouse gas emissions, inhibition, feedback loop, climate change

Introduction

Carbon dioxide (CO_2) receives primary attention as a driver for climate change, but methane (CH_4) and nitrous oxide (N_2O) account for ~20% and 7%, respectively, of the net radiative forcing in the atmosphere [1, 2]. The central objective of the Paris Agreement, which is to hold the global average temperature increase to "well below 2°C above preindustrial levels" [3, 4], cannot be met without controlling CH_4 and N_2O emissions. Global emissions of both CH_4 and N_2O are ultimately controlled by microbial processes [2, 5]; however, human activities have massively disturbed the natural balance of microbial production and consumption of these greenhouse gases [6]. The current estimated annual net atmospheric emission increases of ~51 Tg of CH_4 [7, 8] and 2.2 Tg of N_2O [9] are both predicted to accelerate [1, 10]. The key microbial guilds and biogeochemical processes responsible for CH_4 and N_2O production and consumption are known, and their responses to climate change have been a matter of intense research [11, 12]. One area of considerable uncertainty pertains to positive and negative feedback loops affecting greenhouse gas emissions and

climate [13]. An infamous scenario for a positive feedback loop in response to a warming climate is permafrost thawing, which stimulates the microbial activity and the release of CO_2, CH_4, and N_2O from newly bioavailable carbon and nitrogen pools. The massive release of greenhouse gases will further accelerate radiative forcing and in turn cause more thawing. This example illustrates why a comprehensive understanding of both positive and negative feedback loops is essential. Quantitative information is needed to meaningfully incorporate feedback effects into refined climate models.

Methanogenic archaea (methanogens) drive CH_4 production by utilizing acetate, H_2/CO_2, and methylated compounds as substrates, generating around 1 billion metric tons of CH_4 annually [14, 15]. Approximately, two-thirds of biogenic CH_4 is produced from acetoclastic methanogenesis (i.e. the conversion of acetate to CH_4 and CO_2), with the remaining one-third attributed to hydrogenotrophic CO_2 reduction (hydrogenotrophic pathway) and methylated compound utilization (methylotrophic pathways) [16–20]. While the three major methanogenesis pathways share a core set of enzymes, several mechanistically distinct enzyme
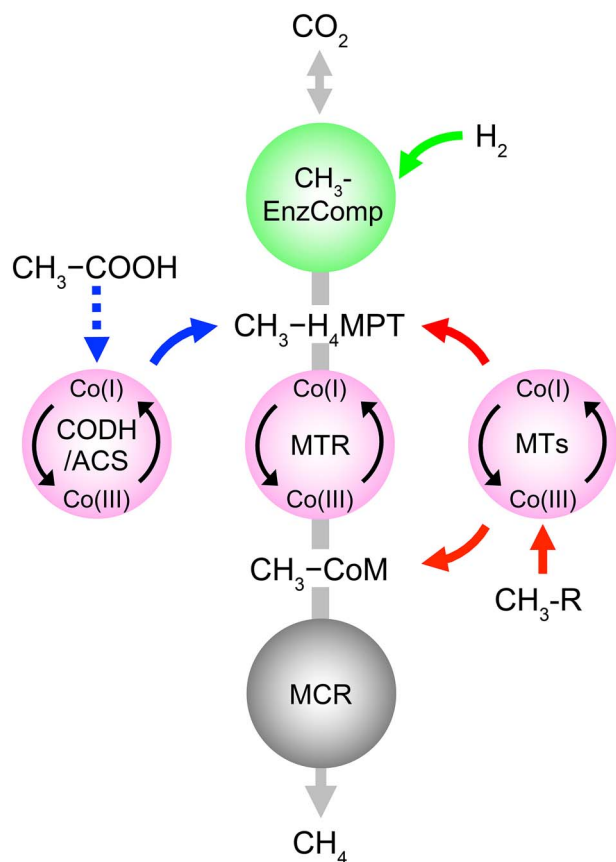
Figure 1. Illustration of the major methanogenic pathways that together account for most of the biogenically produced CH_4 in nature; acetoclastic (left), hydrogenotrophic (top), and methylotrophic (right) conversions channel into the methanogenic pathway; the central circles indicate steps catalyzed by corrinoid-dependent enzyme systems potentially susceptible to N_2O inhibition; abbreviations: CH_3-EnzComp, CH_3-formation enzyme complexes; CH_3-H_4MPT, methyl-tetrahydromethanopterin; MTR, N^5-methyltetrahydromethanopterin: CoM methyltransferase; MTs, substrate-specific methyltransferases; CH_3-R, methylated compounds (e.g. methanol).

systems with corrinoid prosthetic groups (i.e. vitamin B_{12} derivatives) are involved in methyl group transfer reactions, energy conservation, and CH_4 production (Fig. 1) [18, 19, 21].

In hydrogenotrophic methanogenesis, CO_2 is sequentially reduced to a methyl group carried by tetrahydromethanopterin (H_4MPT) with H_2 as electron donor. The corrinoid-dependent N^5-methyltetrahydromethanopterin:CoM methyltransferase (MTR) complex then transfers the methyl group onto another C_1-carrier, coenzyme M, forming CH_3–S–CoM, a step associated with energy conservation, followed by CH_4 production catalyzed by methyl coenzyme M reductase (MCR) [22]. Acetoclastic methanogens produce CH_4 by activating acetate to acetyl-CoA, which is then cleaved by the corrinoid-dependent enzyme system carbon monoxide dehydrogenase/acetyl-CoA synthase (CODH/ACS) to yield an enzyme-bound methyl group and a carbonyl group. The carbonyl moiety is oxidized to CO_2 and the methyl group is transferred to H_4MPT [23]. The MTR complex catalyzes a methyl group transfer to form CH_3–S–CoM, a step associated with energy conservation, before MCR mediates the reduction of the methyl group to CH_4 [16, 24]. Methylotrophic methanogens either directly generate CH_3–S–CoM from methylated compounds (e.g. MeOH) utilizing substrate-specific, corrinoid-dependent MTRs, or

cleave the methyl group from methoxylated compounds (e.g. 2-methoxybenzoate) and form CH_3–CoM via H_4MPT and the MTR complex [25], followed by CH_4 production via MCR. All three methanogenesis pathways utilize corrinoid-dependent enzyme systems for methyl group transfers and have strict requirements for super-reduced Co(I) to generate CH_4 and conserve energy [26, 27]. These features render methanogenesis sensitive to oxidative stress (e.g. fluctuating redox conditions and oxygen intrusion) [19, 28].

N_2O is an even stronger oxidant than oxygen ($E^{o'}(N_2O(g)/N_2(g) = +1.355$ V $> E^{o'}(O_2(g)/H_2O(l) = +0.818$ V), reacts with Co(I), and has been shown to interfere with Co(I) cobamide-dependent enzyme systems [29, 30]. Demonstrated metabolic consequences include ceased corrinoid-dependent methionine biosynthesis and impaired organohalide respiration [31–33]. Based on this information, elevated N_2O in anoxic ecosystems would be expected to inhibit other corrinoid-dependent processes such as methanogenesis; however, available studies investigating the impacts of N_2O on methanogenesis have led to inconsistent N_2O inhibition patterns for axenic methanogen cultures and CH_4 producing microbial communities [34–36]. Laboratory incubations showed that *Methanobacterium bryantii* strain Bab1 grown with H_2/CO_2 ceased CH_4 production in the presence of 95 μM N_2O, whereas *Methanosarcina barkeri* strain MS maintained some methanogenic activity at 10-fold higher N_2O concentrations under the same growth conditions [35]. Different sensitivities to N_2O inhibition were also reported for mixed methanogenic cultures maintained with different substrates. For example, inhibition of CH_4 production in a mixed community bioreactor occurred only at N_2O concentrations exceeding 700 μM [36], whereas 20–28 μM N_2O completely inhibited methanogenic activity in salt marsh sediment and Amazon peatland enrichment cultures [34, 37]. These variable sensitivities to N_2O suggest that inhibition of methanogenesis by N_2O is organism- and possibly substrate-specific; however, the available data are scarce and do not allow a robust, quantitative assessment of N_2O inhibition on methanogenesis from relevant methanogenic substrates [34–36].

N_2O fluxes in soil–water systems have risen sharply due to the intensified use of synthetic N fertilizer in agriculture [6, 9, 38]. As a result, elevated N_2O concentrations occur more frequently in ecosystems with CH_4 production such as rice paddy soils [39], wastewater treatment plants [40], sediments [41], and groundwater aquifers [42]. Also, permafrost thawing accelerates N turnover, releasing large amounts of N_2O [38, 43]. More detailed knowledge about the interactions between N_2O concentrations and methanogenesis is needed to advance the predictive capabilities of climate change impacts on future greenhouse gas emission scenarios. To address the existing knowledge gaps, we assessed the inhibitory effect of N_2O on CH_4 production from major methanogenic substrates in growth experiments with axenic and mixed methanogenic cultures and in whole-cell suspension assays. Using cultures performing acetoclastic, methylotrophic, and/or hydrogenotrophic methanogenesis, we determined kinetic parameters that quantitatively describe N_2O inhibition on methanogenesis.

Materials and methods
Methanogenic cultures and growth inhibition experiments

The methanogenic archaeon *M. barkeri* strain Fusaro metabolizes acetate, H_2/CO_2, and MeOH while employing different, substrate-specific methanogenic pathways. To determine if *M. barkeri*

exhibits varied sensitivities to N_2O, cultures were pregrown with MeOH, H_2/CO_2, or acetate for at least three consecutive transfers before the impact of N_2O on CH_4 production was examined. Also, we analyzed three methanogenic mixed cultures derived from anaerobic digester sludge, which is known to harbor a broad diversity of methanogenic archaea. Three different enrichment cultures from the same source material were obtained with MeOH, H_2/CO_2, or acetate as growth substrate. The mixed cultures were transferred at least six times on the respective substrate and were used to examine the impact of N_2O on CH_4 production from different methanogenic substrates (see Supplemental Information for additional information on the mixed methanogenic cultures). Experiments were performed in triplicate 60-ml glass serum bottles with 30 ml N_2/CO_2 (80/20, v/v) headspace and 30 ml bicarbonate-buffered (50 mM) mineral salt medium (pH 7.2) reduced with 0.2 mM sulfide and 0.2 mM L-cysteine [44]. Acetoclastic, methylotrophic, and hydrogenotrophic cultures received 20 mM acetate, 30 mM MeOH, and 1.24 mmol H_2, respectively. To avoid overpressure in bottles with H_2 as electron donor, the headspace of culture bottles was replaced with 30 ml of filter-sterilized H_2. For *M. barkeri* cultures, 0.1–1.0 ml of N_2O gas (undiluted or 10-fold diluted in N_2) was directly added to the incubation vessels to achieve final aqueous N_2O concentrations of 100 and 200 μM in cultures with MeOH, 50 and 100 μM in cultures with H_2, and 20 and 50 μM in cultures with acetate. For the methanogenic mixed cultures grown with 30 mM MeOH, 30 ml H_2 (1.24 mmol), and 20 mM acetate, 0.5–1.6 ml of 10-fold diluted N_2O gas (in N_2) was introduced to achieve final aqueous phase N_2O concentrations of 10 and 30 μM. More detailed information about N_2O additions and concentration calculations is provided in the Supplemental Methods. All cultures were incubated without agitation at 37°C in the dark with the stoppers facing up, and replicates without N_2O and without inoculum served as positive and negative controls, respectively. CH_4 and N_2O were analyzed throughout the growth experiments by injecting 100 μl headspace samples into an Agilent 3000A Micro gas chromatograph equipped with thermal conductivity detectors and a molecular sieve column and a PLOT Q column for CH_4 and N_2O measurements, respectively.

Whole-cell suspension assays to determine N_2O inhibition constants for CH_4 production

The *M. barkeri* and the methanogenic mixed cultures were first grown in 1.6 l medium and harvested via centrifugation when about two-thirds of the initial substrate (i.e. MeOH, H_2/CO_2, or acetate) had been converted to CH_4, as calculated based on CH_4 production according to Equations (1)–(3) (see below). The cell pellets collected from 1.6 l of medium were washed and suspended in 1.6 ml of reduced mineral salt medium in sealed 2-ml glass vials, resulting in a 1000-fold concentration of the biomass. A 0.2 ml aliquot of the concentrated cell suspension was sacrificed to measure total protein with the Bradford assay [45].

Cell suspension assays were performed at room temperature in 20-ml glass vials flushed with N_2/CO_2 (80/20, v/v) and were sealed with Teflon-lined butyl rubber stoppers held in place with aluminum crimps. The assay vials received a total of 0.9 ml reduced mineral salt medium, 0.1 ml of cell suspension, and increasing concentrations of substrates (i.e. MeOH, H_2, or acetate, with N_2O as indicated in Tables S1–S7). For assay vials receiving H_2 as electron donor, the headspace was replaced with increasing volumes of premixed H_2/CO_2 (4/1, v/v) to achieve H_2 concentrations ranging from 1.2 to 333 μM (Table S3). Small volumes (89–178 μl) of undiluted or 10-fold diluted (in N_2) N_2O were

directly injected into the 20-ml assay vials, what resulted in small pressure changes with negligible impact on the distribution of N_2O between the aqueous phase and the headspace. All cell suspensions were freshly prepared following identical procedures to ensure consistency between independent experiments. Vials that received 0.1 ml of sterile mineral salt medium or 0.1 ml of heat-killed (i.e. autoclaved) cell suspension served as negative controls.

Following 10 min of equilibration, 0.1 ml of cell suspension was added to initiate the assays. Headspace samples (100 μl) were withdrawn with an air-tight syringe with a lock every 30 min over a 3-h incubation period and, for the kinetic experiments, CH_4 was analyzed using an Agilent 7890 GC series gas chromatograph equipped with a flame ionization detector and a DB-624 capillary column (60 m length × 0.32 mm diameter, 1.8 μm film thickness). For each treatment at a fixed initial substrate concentration [S], an initial CH_4 production rate v, normalized to the amount of protein per vial in the unit of nmol CH_4 min^{-1} mg $protein^{-1}$, was determined. The determined rate data were fit into Michaelis–Menten competitive, noncompetitive, and uncompetitive inhibition models (Table S8) to determine the maximum CH_4 production rate V_{max}, the half-velocity constant K_m, and the inhibitory constant K_I of N_2O on CH_4 production from the different substrates. The best-fit inhibition model was chosen based on the highest coefficient of determination (R^2) and the lowest standard deviation of the residuals (Table S9). Each datum point on the Michaelis–Menten plots (Figure 5) represents a CH_4 production rate generated from at least four time points for one substrate concentration [S].

Genomic DNA extraction and 16S ribosomal RNA gene amplicon sequencing

DNA extraction and PCR assays followed established procedures [46] and details are provided in the Supplemental Information. The purified DNA samples were processed and barcoded with primers 341F/785R targeting the V3/V4 region of the prokaryotic 16S rRNA gene [47] following established procedures [48]. The resulting sequence data were analyzed using the QIIME 2 v2021.4 environment [49]. The precise programs and settings are described in the Supplemental Information, and the QIIME 2 pipeline script and custom R file employed to parse results are available at https://github.com/rwmurdoch/methanogens_and_N2O. The raw amplicon library reads were deposited in the Sequence Read Archive (SRA) under accessions SRR19782291 to SRR19782296.

Quantitative real-time PCR and growth yield calculations

Quantitative real-time PCR (qPCR) to enumerate archaeal 16S rRNA genes in *M. barkeri* and methanogenic mixed cultures followed established protocols using primer set Mtgen835F/918R and probe FAM-Mtgen831 (Table S10) [50]. Samples for enumeration of cell numbers were collected at the beginning and at the end of the prolonged growth experiments. Average growth yields of methanogens were calculated from the changes in 16S rRNA gene copy numbers in triplicate culture vessels divided by the total amounts of CH_4 produced over the same time period (Table S11). Reported growth yield (i.e. cells produced per μmol of CH_4 formed) used conversion factors of 3 and 2.5 16S rRNA gene copies per methanogen cell for *M. barkeri* [51] and the enrichment cultures [52], respectively. For comparison with theoretical [53] and reported values from the literature (Table 2), growth yields were also calculated as μg of dry biomass per μmol of CH_4 formed
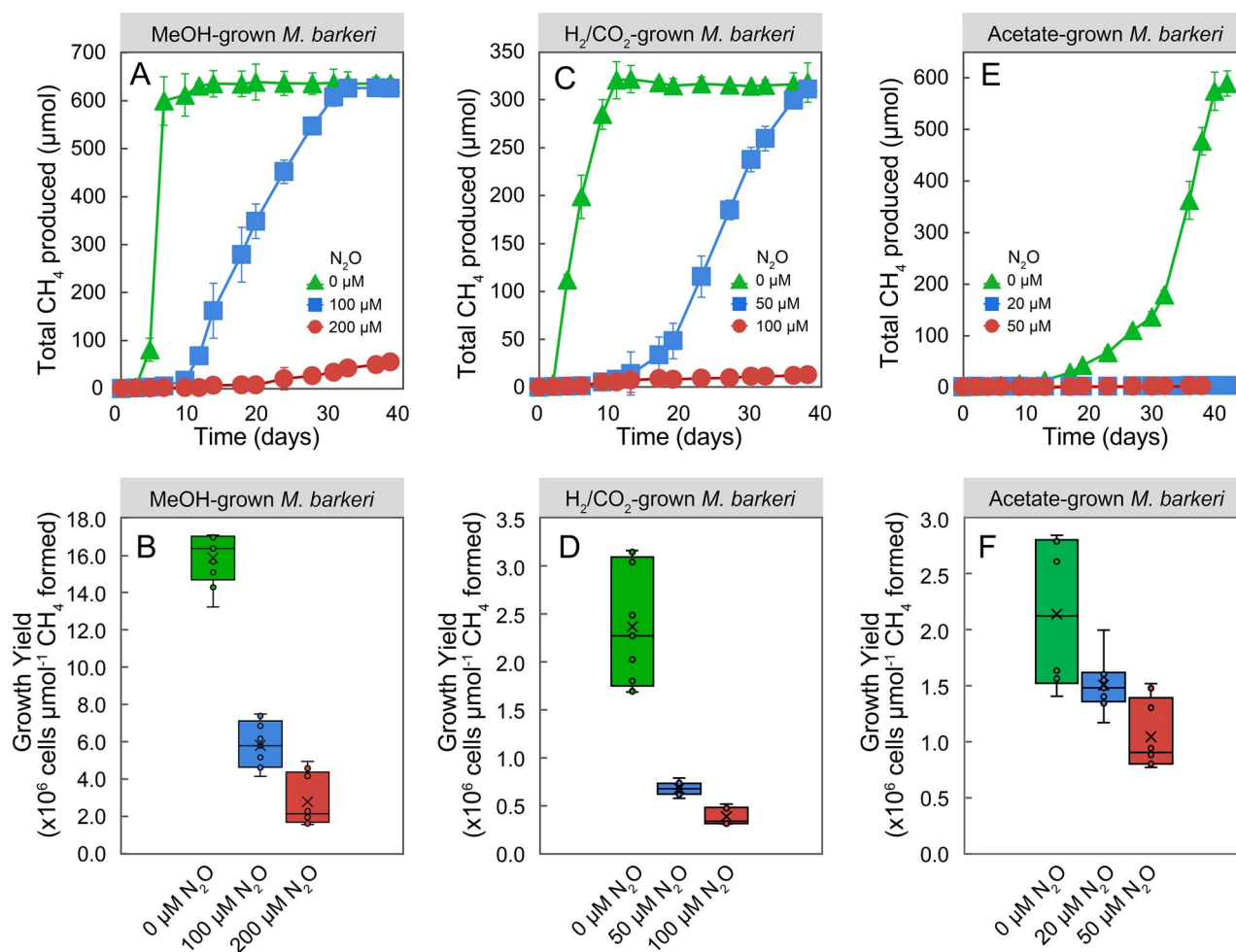
Figure 2. Effect of N_2O on CH_4 production and growth yields in axenic *M. Barkeri* cultures; the upper panels show time courses of CH_4 production in cultures that received MeOH (A), H_2 (C), or acetate (E); the bottom panels display growth yields after 38-day incubation for *M. Barkeri* growing with MeOH (B), H_2 (D), or acetate (F); error bars represent the standard deviation of replicate samples and are not shown when smaller than the symbol size; $n = 3$ for (A), (C), and (E); $n = 9$ (including three technical replicates for triplicate biological samples) for (B), (D), and (F).

making the following assumptions: an average methanogen cell has a volume of 2.5 μm^3 [54] with a density equal to water [55]. The dry cell biomass is 30% of the wet cell biomass [56], and 90% of the dry biomass represents organic material [55].

Results

N_2O has distinct impact on CH_4 production from different methanogenic substrates

In the absence of N_2O, MeOH-grown *M. barkeri* cultures consumed 895 ± 10 μmol of MeOH within a 6-day incubation period and produced 635 ± 34 μmol of CH_4 (Fig. 2A). This stoichiometry closely matched the expected CH_4 production based on Equation (1):

$$4CH_3OH \rightarrow 3CH_4 + CO_2 + 2H_2O \quad \Delta G^o = -105 \text{ kJ mol}^{-1}CH_4 \quad (1)$$

Growth yields of 5.3 × 10^6 ± 0.3 × 10^6 cells per μmol CH_4 were measured for cultures without N_2O (Fig. 2B). By contrast, cultures that received 100 or 200 μM N_2O produced negligible amounts of CH_4 during the initial 6-day incubation period without any apparent growth after 6 days. Following an 11-day lag phase, cultures with 100 μM N_2O started consuming MeOH, and 626 ± 20 μmol of CH_4 were produced following a 38-day incubation period, indicating that 100 μM N_2O delayed, but

did not prevent, CH_4 production from MeOH by *M. barkeri* (Fig. 2A). Although complete conversion of MeOH to CH_4 according to Equation (1) was achieved in the presence of 100 μM N_2O over a prolonged 38-day incubation period, the growth yield decreased by 63.8% ± 7.8% compared to cultures without N_2O, (i.e. 1.9 × 10^6 ± 0.4 x 10^6 vs. 5.3 × 10^6 ± 0.3 × 10^6 cells were produced per μmol of CH_4 formed) (Fig. 2B). In the presence of 200 μM N_2O, only 55 ± 11 μmol of CH_4 were produced over a 38-day incubation period, and the growth yield decreased by over 80% to 0.9 × 10^6 ± 0.4 × 10^6 cells per μmol CH_4, indicating a pronounced inhibitory effect of N_2O on CH_4 production and growth of *M. barkeri*.

More pronounced N_2O inhibition on CH_4 production and growth was observed in *M. barkeri* cultures that received H_2 as electron donor (i.e. hydrogenotrophic methanogenesis). In the absence of N_2O, *M. barkeri* cultures, that received H_2 as electron donor, produced 318 ± 21 μmol of CH_4 from 1.24 mmol of H_2 over an 11-day incubation period, consistent with Equation (2):

$$4H_2 + CO_2 \rightarrow CH_4 + 2H_2O \quad \Delta G^o = -131 \text{ kJ mol}^{-1}CH_4 \quad (2)$$

In the absence of N_2O, a growth yield of 0.8 × 10^6 ± 0.2 × 10^6 cells per μmol CH_4 formed was measured (Fig. 2C and D). In the presence of 50 or 100 μM N_2O, CH_4 production by *M. barkeri*

cultures commenced after prolonged lag phases ranging from 13 to 17 days. At the end of the 38-day incubation period, *M. barkeri* cultures with 50 μM N_2O and produced 311 ± 7 μmol of CH_4. The *M. barkeri* cultures that had received 100 μM N_2O only generated 17 ± 3.2 μmol of CH_4, resulting in a 95% decrease in total CH_4 production compared to cultures without N_2O. The average growth yield in cultures with 50 or 100 μM N_2O decreased by ~70% and 85% to $2.3 \times 10^5 \pm 0.3 \times 10^5$ and $1.2 \times 10^5 \pm 0.3 \times 10^4$ cells per μmol CH_4 formed, respectively, compared to cultures without N_2O.

The most pronounced N_2O inhibition was observed in acetate-fed *M. barkeri* cultures, and 20 μM N_2O severely diminished CH_4 production (Fig. 2E). In the absence of N_2O, *M. barkeri* produced 588 ± 24 μmol of CH_4 from 605 ± 17 μmol of acetate over a 38-day incubation period, consistent with Equation (3):

$$CH_3COO^- + H^+ \rightarrow CH_4 + CO_2 \ \Delta G^{o'} = -35 \text{ kJ mol}^{-1} \text{ CH}_4 \quad (3)$$
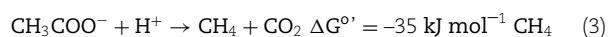
In the presence of 20 or 50 μM N_2O, *M. barkeri* cultures only produced 21.3 ± 4.1 and 20.4 ± 3.8 μmol of CH_4, respectively, a decline of over 96% in total CH_4 production compared to cultures without N_2O over the 38-day incubation period. Acetate-grown *M. barkeri* cultures that had received 20 or 50 μM N_2O generated $1.5 \pm 0.2 \times 10^6$ and $1.0 \pm 0.3 \times 10^6$ cells per μmol of CH_4 produced, decreases of $30.4\% \pm 3.3\%$ and $52.5\% \pm 12.6\%$, respectively, compared to the average yield of $2.1 \times 10^6 \pm 0.7 \times 10^6$ cells per μmol CH_4 in cultures without N_2O (Fig. 2F).

In all culture vessels with observed inhibition of methanogenic activity, N_2O concentrations remained constant throughout the experiment, consistent with the absence of a "*nos*" operon on the genome of *M. barkeri*. Taken together, these results demonstrate that micromolar levels of N_2O inhibit methanogenesis, reduce growth yields of this model methanogen, and further reveal that the inhibition is most pronounced for acetoclastic methanogenesis.

N_2O adversely affects CH_4 production and methanogen growth yields in mixed methanogenic enrichment cultures

To examine the impact of N_2O on mixed methanogen communities, growth and kinetic assays were performed with enrichment cultures derived from digester sludge. Microbial community analysis revealed the presence of diverse methanogen groups known to utilize acetate, H_2/CO_2, and MeOH as substrates, with distinct methanogen taxa prevalent under the different enrichment conditions (Tables S12 and S13). In cultures that received H_2 as electron donor, sequences representing the genus *Methanobacterium* and other unidentified members of the family *Methanobacteriaceae* dominated, whereas in acetate-fed cultures, *Methanosarcina* was the most abundant archaeal taxon. *Methanomethylovorans* was the most abundant archaeal genus in the MeOH-fed cultures, but sequences representing the genus *Methanomassiliicoccus* were also prevalent. 16S rRNA gene amplicons representing six families and four of the known eight orders of methanogens were represented in the examined mixed cultures derived from digester sludge (Fig. 3A and B; Table S12).

Without N_2O addition, the mixed cultures produced 542.6 ± 23.3, 316.5 ± 25.4, and 589.2 ± 33.7 μmol of CH_4 from 0.9 mmol of MeOH, 1.24 mmol of H_2, or 0.6 mmol of acetate, consistent with Equations (1)–(3). When cultures were amended with 10 or 30 μM N_2O, CH_4 production in MeOH-, H_2-, and acetate-fed methanogenic mixed cultures was substantially or completely inhibited (Fig. 4A, C, and E). Even over an extended 42-day incubation period, the presence 10 μM N_2O still repressed the total CH_4 production in MeOH-, H_2-, or acetate-grown mixed cultures by ~60%, 80% and 50%, respectively, compared to incubations without N_2O. With 30 μM N_2O, only negligible amounts of CH_4 were detected in all incubations over a 42-day incubation period. Some N_2O loss was observed in the mixed culture vessels that received H_2/CO_2 or MeOH as substrates, with no more than 20% of the initial amount of N_2O consumed. Taken together, these results demonstrate that N_2O exerts a stronger inhibitory effect on methanogenesis in the mixed cultures harboring diverse methanogen populations than in axenic *M. barkeri* incubations.

Enumeration of total methanogens and total bacteria in the mixed cultures using qPCR revealed that N_2O diminished methanogen growth yields (Fig. 4B, D, and F). The qPCR analysis further revealed significantly decreased ratios of methanogen-to-bacterial 16S rRNA genes in all N_2O-treated cultures (Fig. 3C–E), illustrating that N_2O impacted the methanogen populations much more strongly than the bacterial populations. In the absence of N_2O, the average growth yields of methanogens in the enrichment cultures with MeOH, H_2, or acetate were $0.6 \times 10^7 \pm 0.1 \times 10^7$, $0.6 \times 10^5 \pm 0.3 \times 10^5$, and $1.0 \times 10^6 \pm 0.1 \times 10^6$ cells per μmol of CH_4 formed, respectively. In the presence of 10 μM N_2O, the growth yields of methanogens declined by ~90%, 60%, and 50% in enrichment cultures that received MeOH, H_2, and acetate, respectively (Fig. 4B, D, and F). Only negligible CH_4 production and methanogen growth were measured in all mixed cultures with 30 μM N_2O (Fig. 4B, D, and F). Taken together, the results of the mixed culture studies corroborate that N_2O concentrations in the low micromolar range exhibit pronounced inhibitory effects on hydrogenotrophic, methylotrophic, and acetoclastic methanogenesis in microbial communities.

Kinetic studies confirm potent N_2O inhibition of methane formation rates

Whole-cell suspension assays using *M. barkeri* and the methanogenic mixed cultures were performed to quantitatively assess the inhibitory effects of N_2O on CH_4 production from each methanogenic substrate (Table S1). The Michaelis–Menten single-substrate single-inhibitor model ($R^2 > 0.95$) best explained the trends of CH_4 production rates versus increasing substrate concentrations (Fig. 5). Among all assays with *M. barkeri* and the mixed cultures, maximum CH_4 production rates (i.e. V_{max} values) of acetate-fed cultures were most strongly affected by increasing N_2O concentrations, followed by the H_2- and MeOH-fed cultures (Figs 2 and 3).

In the absence of N_2O, the V_{max} values for CH_4 production in MeOH-, H_2-, or acetate-amended *M. barkeri* cell suspension assays were 440.4 ± 10.2, 138.1 ± 6.9, and 40.8 ± 4.7 nmol CH_4 min^{-1} mg protein^{-1}, respectively (Fig. 5A, Table 1). The addition of N_2O decreased the V_{max} of CH_4 production in MeOH-, H_2-, and acetate-fed *M. barkeri* cell suspension assays to different extents. Rate data determined in *M. barkeri* suspensions assays with MeOH fit the Michaelis–Menten inhibition model best. The V_{max} values declined by ~45% and 57% to 244.1 ± 38.4 and 188.8 ± 32.5 nmol CH_4 min^{-1} mg protein^{-1}, respectively, in the presence of 100 and 200 μM N_2O. The determined inhibitory constant, K_I, of N_2O on methylotrophic CH_4 production was 130.9 ± 4.7 μM in *M. barkeri* cell suspensions (Table 1), indicating that N_2O concentrations around 130 μM reduced the maximum CH_4 production rate (V_{max}) by 50%. More pronounced N_2O inhibition was observed in *M. barkeri* whole-cell suspensions assays using H_2 as the electron donor for CO_2 reduction (Fig. 5B). The addition of 50 and 100 μM
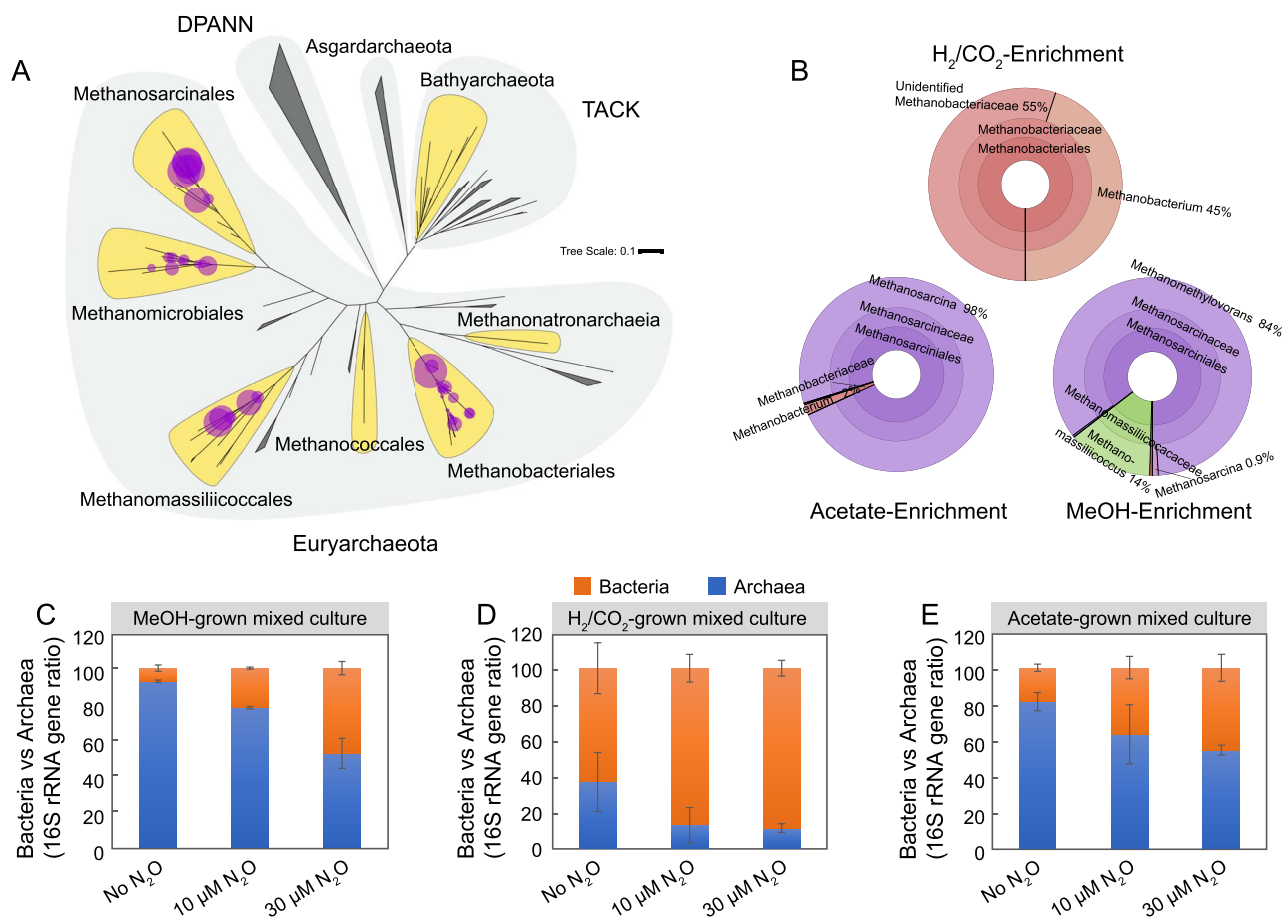
Figure 3. The composition and relative abundances of total sequences representing methanogenic archaea in mixed cultures enriched with acetate, H_2/CO_2, or MeOH; (A) phylogenetic placements of archaeal 16S rRNA gene amplicons detected in the enrichment cultures; the highlighted lobes indicate major clades of archaea known or suspected to produce CH_4; the circles indicate best phylogenetic placements of archaeal taxa identified across all enrichment conditions; the size of the circle is proportional to the number of actual sequence variants (ASVs) detected; large shaded areas indicate archaeal superphyla, including *Diapherotrites*, *Parvarchaeota*, *Aenigmarchaeota*, *Nanohaloarchaeota*, and *Nanoarchaeota* (DPANN) and *Thaumarchaeota*, *Aigarchaeota*, *Crenarchaeota*, and *Korarchaeota* (TACK); see Supplemental Information for details on tree construction and fragment placement methodology; (B) relative abundances of total sequences representing methanogenic archaea in mixed cultures; panels (C) MeOH, (D) H_2/CO_2, and (E) acetate depict qPCR data showing the proportional changes of total bacterial and total archaeal (methanogen) 16S rRNA genes in the mixed cultures without N_2O and in the presence of 10 and 30 μM N_2O; error bars represent the standard deviation of replicate samples ($n = 9$, three technical replicates of triplicate biological samples).

N_2O reduced the V_{max} values in H_2-fed *M. barkeri* cell suspension assays by ~40% and 57% to 82.8 ± 29.5 and 59.9 ± 5.9 nmol of CH_4 min^{-1} mg protein^{-1}, respectively. The model simulation determined a K_I value of 90.6 ± 10.8 μM N_2O (Fig. 5B, Table 1), indicating a stronger inhibition of N_2O on CH_4 production in H_2- versus MeOH-amended *M. barkeri* cell suspension assays. The *M. barkeri* assays with acetate as substrate showed the most pronounced inhibition by N_2O (Fig. 5C, Table 1). In assays amended with 20 and 40 μM N_2O, the V_{max} values decreased by 21% and 44% to 32.1 ± 4.2 and 22.8 ± 2.5 nmol of CH_4 min^{-1} mg protein^{-1}, respectively. From the best-fit inhibition model, a K_I value of 24.8 ± 2.6 μM was determined for N_2O inhibition of acetoclastic methanogenesis in *M. barkeri* cell suspensions. Collectively, the cell suspension assays corroborate strong inhibitory effects of N_2O on methanogenesis, with the kinetics of acetoclastic methanogenesis being most impacted by N_2O.

Similar kinetic responses were observed for whole-cell suspension assays conducted with the methanogenic mixed cultures pregrown with the respective substrates (Fig. 5D–F). In the absence of N_2O, the determined V_{max} values for mixed culture cell

suspension assays that received MeOH, H_2, or acetate were 209.0 ± 4.4, 105.8 ± 3.7, and 22.8 ± 0.7 nmol CH_4 min^{-1} mg protein^{-1}, respectively (Table 1). Notably, the methanogenic mixed cultures were more sensitive to N_2O than axenic *M. barkeri* cultures irrespective of the type of methanogenic substrate provided. In cell suspension assays that received MeOH, the presence of 50 and 100 μM N_2O reduced the V_{max} values by $37.4 \pm 10.8\%$ and $75.4 \pm 21.4\%$, respectively, compared to assays without N_2O. The inhibition model determined a K_I value of 109.9 ± 6.8 μM for N_2O inhibition on CH_4 production in cell suspension assays amended with MeOH (Fig. 5D, Table 1). In H_2-amended cell suspension assays, the presence of 30 and 60 μM N_2O decreased the V_{max} values by 32.3 ± 9.8 and $65.4 \pm 12.9\%$, respectively, compared to assays without N_2O (Fig. 5E, Table 1). The best-fit inhibition model determined a K_I value for N_2O inhibition of 62.1 ± 6.4 μM for CH_4 production in assays that received H_2 as electron donor. Consistent with the observations made with *M. barkeri*, the most pronounced N_2O inhibition on CH_4 production rates was observed in mixed culture cell suspension assays that received acetate as substrate (Fig. 5F). In
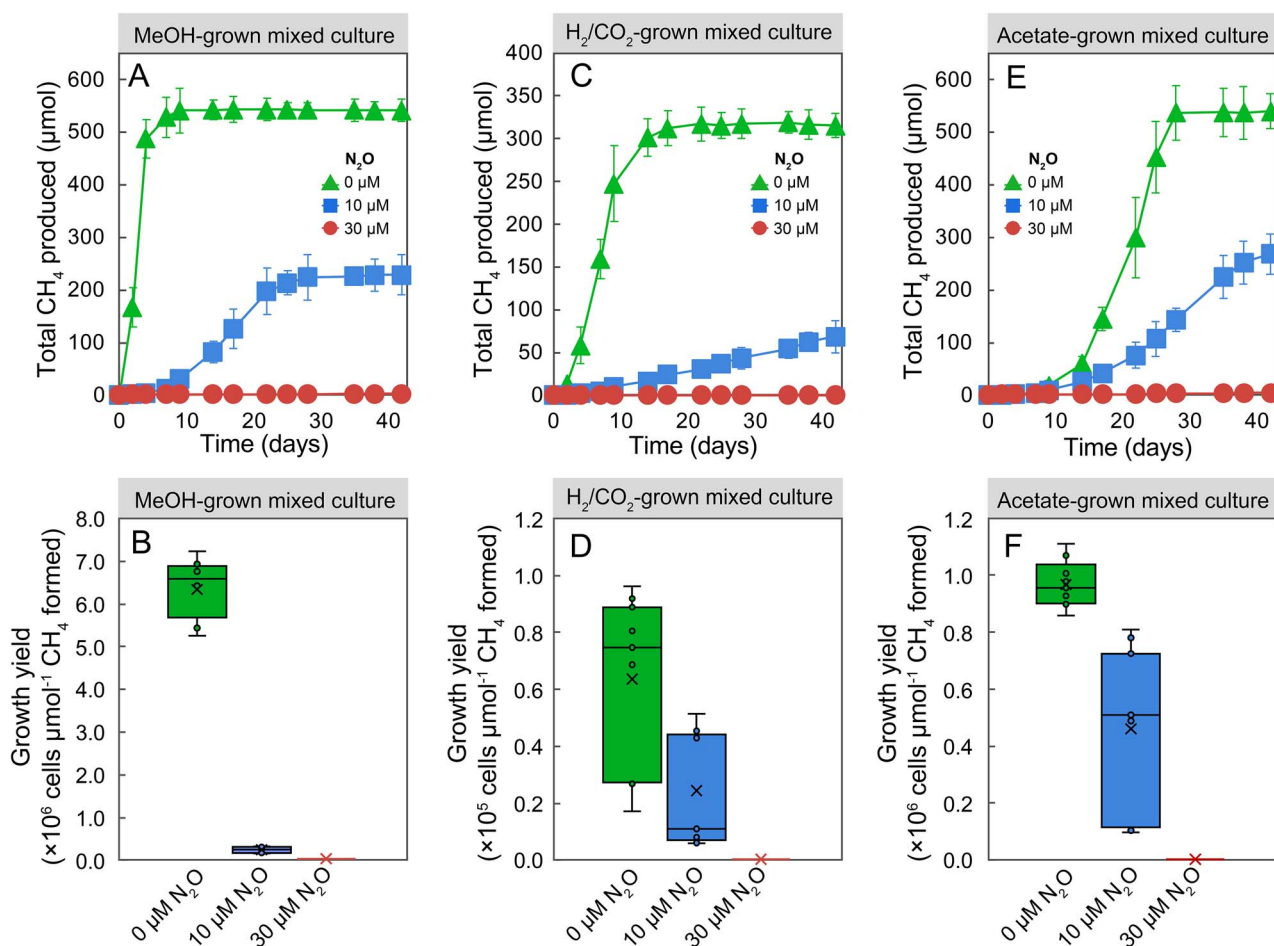
Figure 4. Effects of N_2O on CH_4 production and growth yields in methanogenic mixed cultures enriched with MeOH, H_2, or acetate; the upper panels depict CH_4 production from MeOH (A), H_2 (C), and acetate (E); the bottom panels demonstrate methanogen growth yield differences in cultures amended with MeOH (B), H_2 (D), or acetate (F); error bars represent standard deviation and are not shown when smaller than the symbol size ($n = 3$ for upper panels; $n = 9$ for bottom panels [three technical replicates of triplicate biological samples]).

the presence of 10 and 30 μM N_2O, the V_{max} values in suspension assays with acetate decreased by $38 \pm 7.8\%$ and $74.9 \pm 16.0\%$, respectively, compared to assays without N_2O. Using the best-fit Michaelis–Menten inhibition model, a K_I value of 17.7 ± 1.8 μM was determined for N_2O inhibition of CH_4 production in cell suspension assays with acetate (Table 1).

Taken together, the experimental data demonstrate that dissolved N_2O concentrations in the low μM range (i.e. 20–100 μM) repress CH_4 production and reduce growth yields of *M. barkeri* in axenic culture and of different methanogen guilds in methanogenic mixed cultures. Evaluation of the kinetic data determined in cell suspension assays revealed distinct N_2O inhibition patterns for CH_4 production from acetate, H_2, and MeOH, with the rate of acetoclastic CH_4 production being most sensitive to N_2O inhibition. The K_I values for N_2O inhibition of CH_4 production from key methanogenic substrates ranged between 18 and 130 μM, suggesting N_2O can impact CH_4 production and emissions in diverse ecosystems, including critical zone environments (e.g. thawing permafrost).

Discussion

Microorganisms drive global C and N cycling and ultimately control CH_4 and N_2O production, consumption, and thus emissions to the atmosphere [10, 11, 13]. Predictive climate models must consider the responses of microbial CH_4 and N_2O production

under environmental change scenarios [10, 57]. Quantitative assessment of feedbacks that affect CH_4 production are crucial for refining greenhouse gas emission models. This study investigated the feedback effects between two important greenhouse gases, specifically the inhibitory effect of N_2O on archaeal CH_4 production, to provide quantitative data that link environmental N_2O concentrations with methanogenesis. The findings demonstrate that environmentally relevant, micromolar levels of N_2O suppress CH_4 production and the growth of methanogens. The determined K_I values reveal a concentration-dependent, progressively negative feedback by N_2O on archaeal CH_4 formation rates and the total amounts of CH_4 produced and show that the strength of the inhibition is most pronounced for acetoclastic methanogenesis.

Assuming the current day partial pressure of 335 ppb N_2O in the atmosphere, the theoretical concentration of N_2O in air-equilibrated water should be around 7 nM; however, substantially elevated levels of dissolved N_2O have been observed in groundwater and watersheds [33, 42]. In areas impacted by agricultural activities (e.g. fertilizer application), dissolved groundwater N_2O concentrations can exceed 100 μM [42]. Even in some remote, natural aquatic systems, such as ice-covered Antarctic lakes, N_2O concentrations of up to 86 μM have been reported [58, 59]. N_2O is generated during N cycling and major formation processes include microbial denitrification, ammonia oxidation, and abiotic chemodenitrification [44]. Based on the physiology of the microorganisms (e.g. ammonia oxidizers are
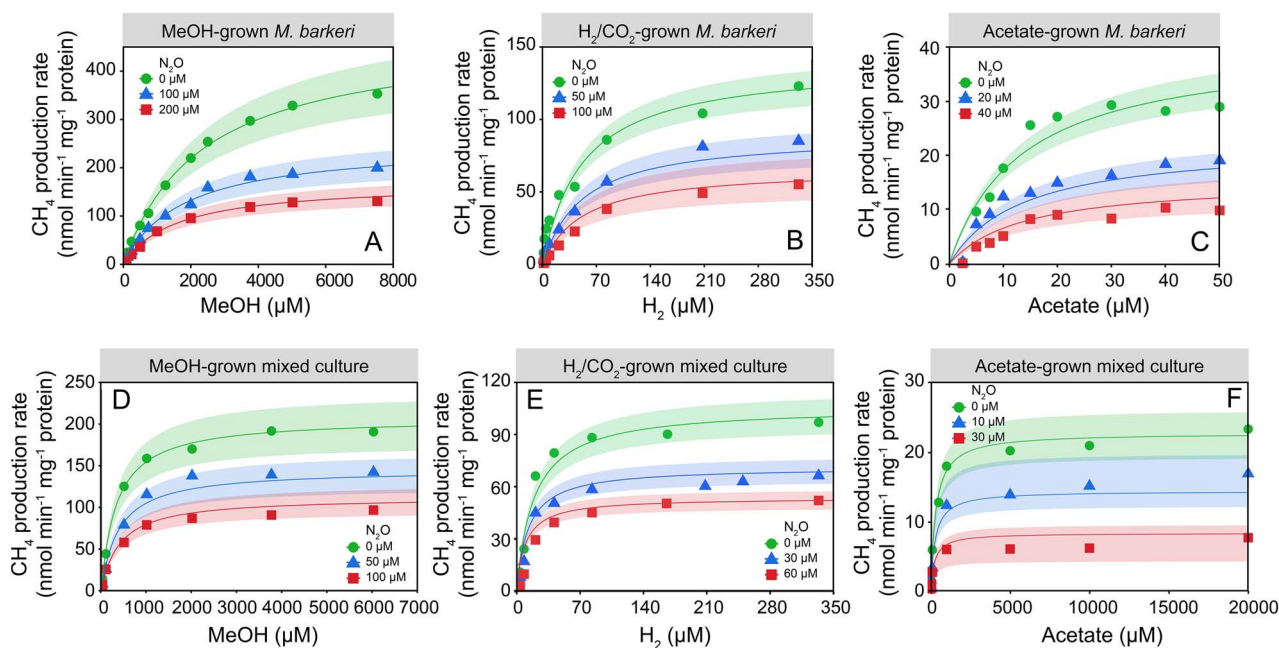
Figure 5. Kinetics of CH$_4$ production from MeOH, H$_2$, and acetate in whole-cell suspension assays of *M. Barkeri* and the methanogenic mixed cultures in the presence of increasing concentrations of N$_2$O; the upper panels show the Michaelis–Menten plots of CH$_4$ production rates versus the respective substrate concentrations in cell suspensions of *M. Barkeri* without and in the presence of increasing N$_2$O concentrations in basal salt medium amended with MeOH (A), H$_2$ (B), or acetate (C); the bottom panels show Michaelis–Menten plots of CH$_4$ production rates versus the respective substrate concentrations in concentrated whole-cell suspensions of the methanogenic mixed cultures without N$_2$O and in the presence of increasing N$_2$O levels in basal salt medium amended with MeOH (D), H$_2$ (E), or acetate (F); the shaded ribbons represent the standard distances (95% confidence interval) between the measured values and the nonlinear regression lines.

strict aerobes) and the thermodynamics of the processes (e.g. nitrate and nitrite reduction are associated with a greater change in Gibbs free energy than methanogenesis), one might argue that N$_2$O formation and methanogenesis are physically separate processes, thus limiting the exposure and inhibitory effects of N$_2$O on methanogens. Such redox stratification does occur; however, most environmental matrices, such as soils, are highly heterogenous and characterized by dynamic spatial and temporal gradients resulting in patchy distribution of redox processes. N$_2$O is water-soluble and, depending on hydrology, can reach other redox zones [60]. Consequently, impacts of elevated N$_2$O on various biogeochemical processes, including those associated with greenhouse gas emissions, are likely. Laboratory studies have reported inhibitory effects of nitrogen oxides (NOx), including N$_2$O, on methanogenesis [34–37, 61, 62]; however, the available data are scarce and no uniform pattern has emerged that would support a quantitative relationship between N$_2$O and microbial CH$_4$ production. Consequently, this negative feedback of N$_2$O on CH$_4$ production has not been considered in greenhouse gas emission models.

The evaluation of N$_2$O inhibition on CH$_4$ production from methanogenic substrates (i.e. MeOH, acetate, and H$_2$/CO$_2$) with both the model methanogen *M. barkeri* and digester sludge-derived mixed methanogenic cultures quantitatively links N$_2$O concentrations with methanogen activity and growth. The growth experiments illustrate that micromolar N$_2$O concentrations affect CH$_4$ production, and the whole-cell suspension assays and kinetic model simulations provide a plausible explanation for the inconsistent literature reports about N$_2$O effects on methanogenesis. Specifically, acetoclastic methanogenesis was most sensitive to N$_2$O (K_I values of 18–25 μM), followed by hydrogenotrophic (K_I 60–90 μM) and methylotrophic methanogenesis (K_I 110–130 μM), indicating that the type of methanogenic substrate utilized affects the sensitivity of methanogens to N$_2$O. N$_2$O

inhibition was significantly more pronounced in methanogenic enrichment cultures than in axenic *M. barkeri* cultures, and 30 μM N$_2$O prevented CH$_4$ production and methanogen growth in the mixed culture experiments regardless of the type of methanogenic substrate utilized. Previous studies support that mixed methanogenic communities are more sensitive to N$_2$O than commonly studied model methanogen isolates [34, 35, 62, 63]. These observations suggest that the axenic methanogen cultures used to elucidate the biochemistry and genetics of methanogenesis may not serve as general models for other features of methanogen biology (e.g. N$_2$O inhibition). The reasons for the reduced sensitivity of axenic versus mixed methanogen cultures to N$_2$O may be a result of long-term adaptation of the isolates to laboratory cultivation, or not-yet-characterized microbe–microbe interaction networks render mixed cultures more susceptible to N$_2$O inhibition. The enrichment cultures used to determine the K_I values for N$_2$O inhibition harbored diverse methanogen groups (Fig. 3A), and kinetic studies (e.g. determination of K_I values for N$_2$O inhibition) with representative isolates of the various lineages are warranted to capture the breadth of methanogen responses to N$_2$O.

Taken together, the low μM range K_I values of N$_2$O that impact methanogenesis suggest major consequences of rising N$_2$O concentrations for C cycling. Of note, the vast majority of the annual ~1 billion metric tons of biogenic CH$_4$ is generated from acetate- and H$_2$-driven CO$_2$ reduction [16–20, 64], the two processes with the lowest observed K_I values for N$_2$O inhibition. It is therefore reasonable to predict that elevated environmental N$_2$O will impact CH$_4$ production and methanogen growth in ecosystems with high bioavailable C and N loads, such as wetlands, sediments, and permafrost soils.

Key enzyme systems involved in CH$_4$ production and energy conservation require cobamide prosthetic groups [65] (Fig. 1). The super-reduced Co(I) form of cobamides is susceptible to

Table 1. Kinetic (V_{max}, K_m) and inhibition (K_I) parameters for CH_4 production from MeOH, H_2, and acetate determined in concentrated whole-cell suspension assays of *M. barkeri* and methanogenic mixed cultures in response to increasing N_2O concentrations.[a]

Culture	Substrate	N_2O (μM)	V_{max} (nmol CH_4 min^{-1} mg protein^{-1})	K_m (μM)	K_I (μM)
M. barkeri	MeOH	0	440.4 ± 10.2	$2.1\ (\pm 0.1) \times 10^3$	130.9 ± 4.7
		100	244.1 ± 38.4		
		200	188.8 ± 32.5		
M. barkeri	H_2	0	138.1 ± 6.9	51.1 ± 7.2	90.6 ± 10.8
		50	82.8 ± 29.5		
		100	59.9 ± 5.9		
M. barkeri	Acetate	0	40.8 ± 4.7	$13.4\ (\pm 2.7) \times 10^3$	24.8 ± 3.1
		20	32.1 ± 4.2		
		50	22.8 ± 2.5		
Mixed culture	MeOH	0	209.0 ± 4.4	359.3 ± 30.8	109.9 ± 6.8
		50	130.8 ± 22.6		
		100	51.4 ± 44.7		
Mixed culture	H_2	0	105.8 ± 3.7	19.0 ± 2.3	62.1 ± 6.4
		30	71.6 ± 10.4		
		60	36.6 ± 13.6		
Mixed culture	Acetate	0	22.8 ± 0.7	302.2 ± 46.2	17.7 ± 1.8
		10	14.1 ± 1.8		
		30	5.7 ± 3.6		

[a]Data listed show results from the best fit Michaelis-Menten single-substrate-single-inhibitor models. Error values represent 95% confidence intervals.

oxidants such as N_2O, a plausible mechanism for the observed inhibition of methanogenesis [29, 34, 63]. The experimental efforts demonstrated that acetoclastic methanogenesis was most sensitive to N_2O, with K_I values in the range of 18–25 μM, indicating that N_2O concentrations in the range of 20 μM would reduce the V_{max} of CH_4 production from acetate by 50%. The K_I values for N_2O inhibition determined for hydrogenotrophic and methylotrophic methanogenesis ranged between 60–90 and 110–130 μM, respectively. The reasons for the apparently substrate-specific K_I values for N_2O inhibition likely reflect differences in the pathways leading to CH_4 production from acetate, H_2/CO_2 and MeOH (Fig. 1). The acetoclastic pathway involves two steps catalyzed by corrinoid-dependent enzyme systems, CODH/ACS and the MTR corrinoid enzyme complex [16, 65]. (Fig. 1), both of which are targets for N_2O inhibition. Distinct cobamide-dependent enzyme systems catalyze the formation of CH_3–CoM in the hydrogenotrophic and the methylotrophic pathways [22, 66]. Both the acetoclastic and hydrogenotrophic pathways depend on the MTR corrinoid enzyme complex to generate CH_3–CoM and to conserve energy [22, 27]. By contrast, methylotrophic methanogens can directly generate CH_3–CoM without the energy-conserving MTR corrinoid enzyme complex from methylated compounds (e.g. MeOH) via a substrate-specific, corrinoid-dependent methyltransferase complex (i.e. MtaA, MtaB, and MtaC in the case of MeOH) [67]. The experimental efforts consistently demonstrated that CH_4 production from acetate and H_2/CO_2 exhibited 7- and 3-fold higher sensitivities, respectively, to N_2O than CH_4 production from MeOH. These findings suggest that N_2O inhibition of methanogenesis is related to the oxidation of the super-reduced Co(I) cobamide, which is essential for the corrinoid enzyme complexes involved in the different methanogenesis pathways. While the differential susceptibilities of pathway-specific corrinoid-dependent enzymatic steps can explain the distinct inhibitory effects of N_2O on CH_4 production via the acetoclastic, hydrogenotrophic, and methylotrophic pathways, detailed enzymatic studies would be needed to assess the responses of individual enzyme systems to N_2O. Kinetic data for the enzymatic regeneration of the super-reduced Co(I) state are lacking, and the rates of reduction may differ between

enzymes and pathways, which could contribute to the observed physiological response of decreased CH_4 production. Recovery from N_2O inhibition was not a focus, but the experimental data indicate partial recovery of methane formation in N_2O-treated axenic and mixed cultures; however, the methanogen growth yields remained lower in N_2O-treated cultures compared to controls without N_2O even over the extended incubation period. Further studies are needed to generate mechanistic insights into modes of recovery from N_2O inhibition.

The presence of N_2O significantly decreased growth yields or completely abolished growth in the examined methanogenic cultures (Table 2). The type of methanogenic substrate utilized determines the fraction of electrons available from electron donor oxidation directed toward cell synthesis and thus governs the growth yields of methanogens [53, 68]. N_2O affects corrinoid-dependent enzymes involved in electron transfer (e.g. the MTR enzyme complex), and it is not surprising that N_2O interferes with energy conservation in methanogens. Consistently, enumeration of methanogen 16S rRNA genes at the termination of all growth experiments illustrated that N_2O not only negatively impacted CH_4 production but also methanogen growth yields. An alternate explanation for the reduced methanogen growth yields in the mixed cultures exposed to N_2O could be competition for electron donor (e.g. H_2); however, the sequencing and the qPCR data do not support this hypothesis, and N_2O inhibition explains the decline of methanogens and the changes of methanogen-to-bacteria ratios. The measured methanogen growth yield data in the absence of N_2O were on par with reported experimental data and closely matched the theoretical values (i.e. yields calculated based on thermodynamics) (Table 2). One exception were the growth yields measured in H_2/CO_2-fed *M. barkeri* cultures, which were ~10-fold lower than data reported in the literature. The most pronounced growth suppression was observed in the mixed methanogenic cultures, where 30 μM N_2O was sufficient to prevent the growth of methanogenic archaea. Collectively, the data show that micromolar concentrations of N_2O decrease or abolish CH_4 production, reduce methanogen growth yields, and exhibit progressively negative feedback on microbial CH_4 production.

Table 2. Comparison of growth yields of methanogens utilizing different substrates with values collected from the peer-reviewed literature and calculated values based on thermodynamics and bioenergetic principles.

Cultures	Substrates	N$_2$O (μM)	Growth yield (μg organic matter per μmol CH$_4$ formed)		
			Measured[a]	Predicted from thermodynamics[b]	Range (references)
M. barkeri	MeOH	0	3.57 ± 0.32	5.2	3.3–6.4 ([71, 72])
	MeOH	100	1.30 ± 0.28		
	MeOH	200	0.62 ± 0.03		
	H$_2$	0	0.53 ± 0.14	3.6	5.4–8.6 ([73])
	H$_2$	50	0.15 ± 0.02		
	H$_2$	100	0.08 ± 0.02		
	Acetate	0	1.45 ± 0.46	2.1	1.4–5.7 ([74])
	Acetate	20	1.02 ± 0.16		
	Acetate	50	0.70 ± 0.02		
Mixed methanogenic cultures	MeOH	0	4.30 ± 0.56	5.2	3.3–6.4 ([72])
	MeOH	10	0.14 ± 0.05		
	MeOH	30	NA		
	H$_2$	0	0.43 ± 0.05	3.6	1.3–7.2 ([14])
	H$_2$	10	0.16 ± 0.01		
	H$_2$	30	NA		
	Acetate	0	0.65 ± 0.05	2.1	1.4–5.7 ([23, 64, 75])
	Acetate	10	0.31 ± 0.02		
	Acetate	30	NA		

[a]Cell numbers were determined with qPCR. Because *M. barkeri* has three copies of the 16S rRNA gene, the qPCR results were divided by a factor of three to obtain cell numbers. Calculation of methanogen cell numbers in the mixed cultures assumed an average 16S rRNA gene content of 2.5. [b]Theoretical values calculated in this study based on thermodynamics and published information [53].

Microbial processes are strongly influenced by environmental factors and their responses to climate change vary both spatially and temporally [11, 69]. To improve the predictive power of climate models and potentially justify the application of biotechnological approaches for managing greenhouse gas emissions, interactions and feedbacks between relevant biotic/abiotic processes must be understood and quantitatively captured [70]. Attempts have been made to include microbial data (i.e. biomass, enzyme, and growth kinetics) to improve climate models [70], but the incorporation of multifactorial, multidirectional, and often nonlinear biotic/abiotic feedbacks underlying the global CH$_4$ and N$_2$O budgets is challenging and requires robust quantitative data. The determined K_I values for N$_2$O inhibition of methanogenesis reveal a relevant negative feedback effect on CH$_4$ emissions, and the new quantitative information generates opportunities to refine CH$_4$ emission models.

Supplementary material

Supplementary material is available at *The ISME Journal* online.

Conflicts of interest

The authors declare no competing interests.

Funding

Data availability

All data generated or analyzed during this study are included in this published article and its supplementary information files. The raw amplicon library reads are available in the SRA repository.

References

1. Intergovernmental Panel on Climate Change (IPCC). Stocker TF (ed.), *Climate change 2013: the physical science basis. Working Group I contribution to the fifth assessment report of the Intergovernmental Panel on Climate Change.* New York: Cambridge University Press, 2013. https://doi.org/10.1017/CBO9781107415324

2. Intergovernmental Panel on Climate Change (IPCC). *Global Warming of 1.5°C: IPCC Special Report on Impacts of Global Warming of 1.5°C above Pre-Industrial Levels in Context of Strengthening Response to Climate Change, Sustainable Development, and Efforts to Eradicate Poverty.* Cambridge: Cambridge University Press, 2018. https://www.ipcc.ch/sr15/

3. United Nations Framework Convention on Climate Change (UNFCCC). *Adoption of the Paris Agreement. Report No. FCCC/CP/2015/L.9/Rev.1.* Geneva: United Nations, 2015. https://unfccc.int/resource/docs/2015/cop21/eng/l09r01.pdf

4. Intergovernmental Panel on Climate Change (IPCC). Shukla PR (ed.), *Climate Change and Land: An IPCC Special Report on Climate Change, Desertification, Land Degradation, Sustainable Land Management, Food Security, and Greenhouse Gas Fluxes in Terrestrial Ecosystems*, Geneva, Switzerland, 2019). https://www.ipcc.ch/srccl/download/.

5. Luan J, Wu J, Liu S *et al.* Soil nitrogen determines greenhouse gas emissions from northern peatlands under concurrent warming and vegetation shifting. *Commun Biol* 2019;**2**:132. https://doi.org/10.1038/s42003-019-0370-1

6. Parn J, Verhoeven JTA, Butterbach-Bahl K *et al.* Nitrogen-rich organic soils under warm well-drained conditions are global nitrous oxide emission hotspots. *Nat Commun* 2018;**9**:1135. https://doi.org/10.1038/s41467-018-03540-1

7. Reay DS, Smith P, Christensen TR *et al.* Methane and global environmental change. *Annu Rev Environ Resour* 2018;**43**:165–92. https://doi.org/10.1146/annurev-environ-102017-030154

8. Jackson RB, Saunois M, Bousquet P *et al.* Increasing anthropogenic methane emissions arise equally from agricultural and

fossil fuel sources. *Environ Res Lett* 2020;**15**:071002. https://doi.org/10.1088/1748-9326/ab9ed2

9. Tian H, Xu R, Canadell JG *et al.* A comprehensive quantification of global nitrous oxide sources and sinks. *Nature* 2020;**586**: 248–56. https://doi.org/10.1038/s41586-020-2780-0

10. Cavicchioli R, Ripple WJ, Timmis KN *et al.* Scientists' warning to humanity: microorganisms and climate change. *Nat Rev Microbiol.* 2019;**17**:569–86. https://doi.org/10.1038/s41579-019-0222-5

11. Singh BK, Bardgett RD, Smith P *et al.* Microorganisms and climate change: terrestrial feedbacks and mitigation options. *Nat Rev Microbiol.* 2010;**8**:779–90. https://doi.org/10.1038/nrmicro2439

12. Stein LY. The long-term relationship between microbial metabolism and greenhouse gases. *Trends Microbiol* 2020;**28**: 500–11. https://doi.org/10.1016/j.tim.2020.01.006

13. Jansson JK, Hofmockel KS. Soil microbiomes and climate change. *Nat Rev Microbiol* 2020;**18**(1):35–46. https://doi.org/10.1038/s41579-019-0265-7

14. Thauer RK, Kaster AK, Seedorf H *et al.* Methanogenic archaea: ecologically relevant differences in energy conservation. *Nat Rev Microbiol.* 2008;**6**:579–91. https://doi.org/10.1038/nrmicro1931

15. Evans PN, Boyd JA, Leu AO *et al.* An evolving view of methane metabolism in the archaea. *Nat Rev Microbiol* 2019;**17**:219–32. https://doi.org/10.1038/s41579-018-0136-7

16. Ferry JG. Acetate-based methane production. In: Wall JD, Harwood CS, Demain A (eds.), *Bioenergy*. Washington, DC. ASM Press: Wiley Online Library, 2008.

17. Lessner DJ. *Methanogenesis Biochemistry*. In eLS, John Wiley & Sons Ltd, Hoboken, NJ, USA, 2009.

18. Ferry JG. Fundamentals of methanogenic pathways that are key to the biomethanation of complex biomass. *Curr Opin Struct Biol* 2011;**22**:351–7. https://doi.org/10.1016/j.copbio.2011.04.011

19. Lyu Z, Shao N, Akinyemi T *et al.* Methanogenesis. *Curr Biol* 2018;**28**:R727–32. https://doi.org/10.1016/j.cub.2018.05.021

20. Carr SA, Schubotz F, Dunbar RB *et al.* Acetoclastic *Methanosaeta* are dominant methanogens in organic-rich Antarctic marine sediments. *ISME J* 2018;**12**:330–42. https://doi.org/10.1038/ismej.2017.150

21. Goetzl S, Jeoung JH, Hennig SE *et al.* Structural basis for electron and methyl-group transfer in a methyltransferase system operating in the reductive acetyl-CoA pathway. *J Mol Biol* 2011;**411**: 96–109. https://doi.org/10.1016/j.jmb.2011.05.025

22. Welander PV, Metcalf WW. Loss of the *mtr* operon in *Methanosarcina* blocks growth on methanol, but not methanogenesis, and reveals an unknown methanogenic pathway. *Proc Natl Acad Sci USA* 2005;**102**:10664–9. https://doi.org/10.1073/pnas.0502623102

23. Prakash D, Chauhan SS, Ferry JG. Life on the thermodynamic edge: respiratory growth of an acetotrophic methanogen. *Sci Adv* 2019;**5**:eaaw9059. https://doi.org/10.1126/sciadv.aaw9059

24. Borrel G, Adam PS, Gribaldo S. Methanogenesis and the wood-Ljungdahl pathway: an ancient, versatile, and fragile association. *Genome Biol Evol* 2016;**8**:1706–11. https://doi.org/10.1093/gbe/evw114

25. Kurth JM, Nobu MK, Tamaki H *et al.* Methanogenic archaea use a bacteria-like methyltransferase system to demethoxylate aromatic compounds. *ISME J* 2021;**15**:3549–65. https://doi.org/10.1038/s41396-021-01025-6

26. Thauer RK, Kaster AK, Goenrich M *et al.* Hydrogenases from methanogenic archaea, nickel, a novel cofactor, and H_2 storage. *Annu Rev Biochem* 2010;**79**:507–36. https://doi.org/10.1146/annurev.biochem.030508.152103

27. Thauer RK. The Wolfe cycle comes full circle. *Proc Natl Acad Sci USA* 2012;**109**:15084–5. https://doi.org/10.1073/pnas.1213193109

28. Richter N, Zepeck F, Kroutil W. Cobalamin-dependent enzymatic O-, N-, and S-demethylation. *Trends Biotechnol* 2015;**33**: 371–3. https://doi.org/10.1016/j.tibtech.2015.03.011

29. Banks RGS, Henderson RJ, Pratt JM. Reactions of gases in solution. Part III. Some reactions of nitrous oxide with transition-metal complexes. *J Chem Soc Sec A* 1968;**0**:2886–9. https://doi.org/10.1039/j19680002886

30. Blackburn R, Kyaw M, Swallow AJ. Reaction of cob(I)alamin with nitrous oxide and cob(III)alamin. *J Chem Soc, Faraday Trans I* 1977;**73**:250–5. https://doi.org/10.1039/f19777300250

31. Drummond JT, Matthews RG. Nitrous oxide inactivation of cobalamin-dependent methionine synthase from *Escherichia coli*: characterization of the damage to the enzyme and prosthetic group. *Biochemistry* 1994;**33**:3742–50. https://doi.org/10.1021/bi00178a034

32. Drummond JT, Matthews RG. Nitrous oxide degradation by cobalamin-dependent methionine synthase: characterization of the reactants and products in the inactivation reaction. *Biochemistry* 1994;**33**:3732–41. https://doi.org/10.1021/bi00178a033

33. Yin Y, Yan J, Chen G *et al.* Nitrous oxide is a potent inhibitor of bacterial reductive dechlorination. *Environ Sci Technol* 2018;**53**: 692–701. https://doi.org/10.1021/acs.est.8b05871

34. Balderston WL, Payne WJ. Inhibition of methanogenesis in salt marsh sediments and whole-cell suspensions of methanogenic bacteria by nitrogen oxides. *Appl Environ Microbiol* 1976;**32**:264–9. https://doi.org/10.1128/aem.32.2.264-269.1976

35. Klüber HD, Conrad R. Inhibitory effects of nitrate, nitrite, NO and N_2O on methanogenesis by *Methanosarcina barkeri* and *Methanobacterium bryantii*. *FEMS Microbiol Ecol* 1998;**25**:331–9. https://doi.org/10.1016/S0168-6496(97)00102-5

36. Tugtas AE, Pavlostathis SG. Inhibitory effects of nitrogen oxides on a mixed methanogenic culture. *Biotechnol Bioeng* 2007;**96**: 444–55. https://doi.org/10.1002/bit.21105

37. Buessecker S, Zamora Z, Sarno AF *et al.* Microbial communities and interactions of nitrogen oxides with methanogenesis in diverse peatlands of the Amazon basin. *Front Microbiol* 2021;**12**:p. 659079. https://doi.org/10.3389/fmicb.2021.659079

38. Elberling B, Christiansen HH, Hansen BU. High nitrous oxide production from thawing permafrost. *Nat Geosci* 2010;**3**:332–5. https://doi.org/10.1038/ngeo803

39. Carlson KM, Gerber JS, Mueller ND *et al.* Greenhouse gas emissions intensity of global croplands. *Nat Clim Chang* 2016;**7**:63–8. https://doi.org/10.1038/nclimate3158

40. Campos JL, Valenzuela-Heredia D, Pedrouso A *et al.* Greenhouse gases emissions from wastewater treatment plants: minimization, treatment, and prevention. *J Chem* 2016;**2016**:1–12. https://doi.org/10.1155/2016/3796352

41. Davidson TA, Audet J, Svenning JC *et al.* Eutrophication effects on greenhouse gas fluxes from shallow-lake mesocosms override those of climate warming. *Glob Change Biol* 2015;**21**:4449–63. https://doi.org/10.1111/gcb.13062

42. Jurado A, Borges AV, Brouyere S. Dynamics and emissions of N_2O in groundwater: a review. *Sci Total Environ* 2017;**584-585**:207–18. https://doi.org/10.1016/j.scitotenv.2017.01.127

43. Harris E, Yu L, Wang YP *et al.* Warming and redistribution of nitrogen inputs drive an increase in terrestrial nitrous oxide emission factor. *Nat Commun* 2022;**13**:4310. https://doi.org/10.1038/s41467-022-32001-z

44. Onley JR, Ahsan S, Sanford RA *et al.* Denitrification by *Anaeromyxobacter dehalogenans*, a common soil bacterium lacking the nitrite reductase genes *nirS* and *nirK*. *Appl Environ Microbiol* 2018;**84**:e01985–17. https://doi.org/10.1128/AEM.01985-17

45. Bradford MM. A rapid and sensitive method for the quantitation of microgram quantities of protein utilizing the principle of

protein-dye binding. *Anal Biochem* 1976;**72**:248–54. https://doi.org/10.1016/0003-2697(76)90527-3

46. Ritalahti KM, Amos BK, Sung Y *et al.* Quantitative PCR targeting 16S rRNA and reductive dehalogenase genes simultaneously monitors multiple *Dehalococcoides* strains. *Appl Environ Microbiol* 2006;**72**:2765–74. https://doi.org/10.1128/AEM.72.4.2765-2774.2006

47. Klindworth A, Pruesse E, Schweer T *et al.* Evaluation of general 16S ribosomal RNA gene PCR primers for classical and next-generation sequencing-based diversity studies. *Nucleic Acids Res* 2013;**41**(1):e1–1. https://doi.org/10.1093/nar/gks808

48. Caporaso JG, Lauber CL, Walters WA *et al.* Global patterns of 16S rRNA diversity at a depth of millions of sequences per sample. *Proc Natl Acad Sci USA* 2011;**108**:4516–22. https://doi.org/10.1073/pnas.1000080107

49. Bolyen E, Rideout JR, Dillon MR *et al.* Reproducible, interactive, scalable and extensible microbiome data science using QIIME 2. *Nat Biotechnol* 2019;**37**:852–7. https://doi.org/10.1038/s41587-019-0209-9

50. Kleindienst S, Chourey K, Chen G *et al.* Proteogenomics reveals novel reductive dehalogenases and methyltransferases expressed during anaerobic dichloromethane metabolism. *Appl Environ Microbiol* 2019;**85**:e02768–18. https://doi.org/10.1128/AEM.02768-18

51. Maeder DL, Anderson I, Brettin TS *et al.* The *Methanosarcina barkeri* genome: comparative analysis with *Methanosarcina acetivorans* and *Methanosarcina mazei* reveals extensive rearrangement within methanosarcinal genomes. *J Bacteriol* 2006;**188**:7922–31. https://doi.org/10.1128/JB.00810-06

52. Sun D-L, Jiang X, Wu QL *et al.* Intragenomic heterogeneity of 16S rRNA genes causes overestimation of prokaryotic diversity. *Appl Environ Microbiol* 2013;**79**:5962–9. https://doi.org/10.1128/AEM.01282-13

53. Rittmann BE, McCarty PL. *Environmental Biotechnology: Principles and Applications*. New York: McGraw-Hill, 2001

54. Blohs M, Moissl-Eichinger C, Mahnert A, *et al.* Archaea – an introduction. In: Schmidt TM (ed.), *Encyclopedia of Microbiology (Fourth Edition)*. Oxford: Academic Press; 2019, p. 243–52. https://doi.org/10.1016/B978-0-12-809633-8.20884-4

55. Duhamel M, Edwards EA. Growth and yields of dechlorinators, acetogens, and methanogens during reductive dechlorination of chlorinated ethenes and dihaloelimination of 1,2-dichloroethane. *Environ Sci Technol* 2007;**41**:2303–10. https://doi.org/10.1021/es062010r

56. Bratbak G, Dundas I. Bacterial dry matter content and biomass estimations. *Appl Environ Microbiol* 1984;**48**:755–7. https://doi.org/10.1128/aem.48.4.755-757.1984

57. Guo X, Gao Q, Yuan M *et al.* Gene-informed decomposition model predicts lower soil carbon loss due to persistent microbial adaptation to warming. *Nat Commun* 2020;**11**:4897. https://doi.org/10.1038/s41467-020-18706-z

58. Priscu JC, Christner BC, Dore JE *et al.* Supersaturated N_2O in a perennially ice-covered Antarctic lake: molecular and stable isotopic evidence for a biogeochemical relict. *Limnol Oceanogr* 2008;**53**:2439–50. https://doi.org/10.4319/lo.2008.53.6.2439

59. Murray AE, Kenig F, Fritsen CH *et al.* Microbial life at −13 °C in the brine of an ice-sealed Antarctic lake. *Proc Natl Acad Sci USA* 2012;**109**:20626–31. https://doi.org/10.1073/pnas.1208607109

60. Priscu JC. The biogeochemistry of nitrous oxide in permanently ice-covered lakes of the McMurdo dry valleys. *Antarctica Glob Chang Biol* 1997;**3**:301–15. https://doi.org/10.1046/j.1365-2486.1997.00147.x

61. Clarens M, Bernet N, Delgenès J-P *et al.* Effects of nitrogen oxides and denitrification by *Pseudomonas stutzeri* on acetotrophic methanogenesis by *Methanosarcina mazei*. *FEMS Microbiol Ecol* 1998;**25**:271–6. https://doi.org/10.1111/j.1574-6941.1998.tb00479.x

62. Klüber HD, Conrad R. Effects of nitrate, nitrite, NO and N_2O on methanogenesis and other redox processes in anoxic rice field soil. *FEMS Microbiol Ecol* 1998;**25**:301–19. https://doi.org/10.1016/S0168-6496(98)00011-7

63. Fischer R, Thauer RK. Methanogenesis from acetate in cell extracts of *Methanosarcina barkeri*: isotope exchange between CO_2 and the carbonyl group of acetyl-CoA, and the role of H_2. *Arch Microbiol* 1990;**153**:156–62. https://doi.org/10.1007/BF00247814

64. Welte C, Deppenmeier U. Bioenergetics and anaerobic respiratory chains of aceticlastic methanogens. *Biochim Biophys Acta* 2014;**1837**:1130–47. https://doi.org/10.1016/j.bbabio.2013.12.002

65. Banerjee R, Ragsdale SW. The many faces of vitamin B_{12}: catalysis by cobalamin-dependent enzymes. *Annu Rev Biochem* 2003;**72**:209–47. https://doi.org/10.1146/annurev.biochem.72.121801.161828

66. Mand TD, Metcalf WW. Energy conservation and hydrogenase function in methanogenic archaea, in particular the genus *Methanosarcina*. *Microbiol Mol Bio Rev* 2019;**83**:e00020–19. https://doi.org/10.1128/MMBR.00020-19

67. Welander PV, Metcalf WW. Mutagenesis of the C1 oxidation pathway in *Methanosarcina barkeri*: new insights into the Mtr/Mer bypass pathway. *J Bacteriol* 2008;**190**:1928–36. https://doi.org/10.1128/JB.01424-07

68. Karadagli F, Rittmann BE. Kinetic characterization of *Methanobacterium bryantii* M.o.H. *Environ Sci Technol* 2005;**39**:4900–5. https://doi.org/10.1021/es047993b

69. Arneth A, Harrison SP, Zaehle S *et al.* Terrestrial biogeochemical feedbacks in the climate system. *Nat Geosci* 2010;**3**:525–32. https://doi.org/10.1038/ngeo905

70. McCalley CK, Woodcroft BJ, Hodgkins SB *et al.* Methane dynamics regulated by microbial community response to permafrost thaw. *Nature* 2014;**514**:478–81. https://doi.org/10.1038/nature13798

71. Hippe H, Caspari D, Fiebig K *et al.* Utilization of trimethylamine and other N-methyl compounds for growth and methane formation by *Methanosarcina barkeri*. *Proc Natl Acad Sci USA* 1979;**76**(1):494–8. https://doi.org/10.1073/pnas.76.1.494

72. Müller V, Blaut M, Gottschalk G. Utilization of methanol plus hydrogen by *Methanosarcina barkeri* for methanogenesis and growth. *Appl Environ Microbiol* 1986;**52**:269–74. https://doi.org/10.1128/aem.52.2.269-274.1986

73. Londry KL, Dawson KG, Grover HD *et al.* Stable carbon isotope fractionation between substrates and products of *Methanosarcina barkeri*. *Organic Geochem* 2008;**39**:608–21. https://doi.org/10.1016/j.orggeochem.2008.03.002

74. Peinemann S, Müller V, Blaut M *et al.* Bioenergetics of methanogenesis from acetate by *Methanosarcina barkeri*. *J Bacteriol* 1988;**170**:1369–72. https://doi.org/10.1128/jb.170.3.1369-1372.1988

75. Feist AM, Scholten JC, Palsson BO *et al.* Modeling methanogenesis with a genome-scale metabolic reconstruction of *Methanosarcina barkeri*. *Mol Syst Biol* 2006;**2**:0004. https://doi.org/10.1038/msb4100046